https://doi.org/10.5194/egusphere-2025-623
Preprint. Discussion started: 21 February 2025


# Quantification of anthropogenic and marine sources to atmospheric mercury over the marginal seas of China and impact assessment on the sea-air exchange of mercury

Xiaofei Qin[1], Hao Li[2], Jia Chen[3], Junjie Wei[4,5], Hao Ding[4,5], Xiaohao Wang[3], Guochen Wang[2], Chengfeng Liu[2], Da Lu[2], Shengqian Zhou[2], Haowen Li[2], Yucheng Zhu[2], Ziwei Liu[2], Qingyan Fu[6], Juntao Huo[3], Yanfen Lin[3], Congrui Deng[2], Yisheng Zhang[1*], Kan Huang[2, 7, 8*]

[1]School of Environmental and Municipal Engineering, Qingdao University of Technology, Qingdao, China

[2]Shanghai Key Laboratory of Atmospheric Particle Pollution and Prevention (LAP[3]), National Observations and Research Station for Wetland Ecosystems of the Yangtze Estuary, Department of Environmental Science and Engineering, Fudan University, Shanghai, China

[3]Shanghai Environment Monitoring Center, Shanghai, China

[4]Key Laboratory of Environmental Pollution Control Technology of Zhejiang Province, Hangzhou, Zhejiang, China

[5]Environmental Science Research & Design Institute of Zhejiang Province, Hangzhou, Zhejiang, China

[6]Shanghai Academy of Environmental Sciences, Shanghai, China

[7]Institute of Eco-Chongming, Shanghai, China

[8]IRDR ICoE on Risk Interconnectivity and Governance on Weather/Climate Extremes Impact and Public Health, Fudan University, Shanghai, China

Correspondence: huangkan@fudan.edu.cn (Kan Huang); doctorzys@163.com (Yisheng Zhang)

**Abstract**

Mercury in the atmosphere is a crucial environmental concern due to its toxicity and ability to travel long distances. In the marginal seas, the contributions of terrestrial anthropogenic vs. natural sources on atmospheric mercury have been rarely quantified and their roles in mercury sea-air exchange are

https://doi.org/10.5194/egusphere-2025-623
Preprint. Discussion started: 21 February 2025


not well understood. To address this issue, this study integrated observations from island, cruise, and inland campaigns. Positive correlations were observed between total gaseous mercury (TGM) concentrations and environmental parameters such as temperature, relative humidity, and wind speed, indicating the significant influence of natural sources on atmospheric mercury in the marine environment. The application of the TGM/BC (black carbon) ratio underscored the effects of continental outflows. By utilizing a receptor model and linear regression analysis, a robust method was developed to quantitatively estimate the contribution of anthropogenic and natural sources to TGM. Anthropogenic sources accounted for an average of 59%, 38%, and 26% of TGM over the Bohai Sea, Yellow Sea, and East China Sea, respectively. The sea-air exchange fluxes of mercury were estimated as 0.17±0.38, 1.10±1.34, and 3.44±3.24 ng $m^{-2}$ $h^{-1}$ over the three seas above, respectively. Upon omitting the contributions of anthropogenic sources, the sea-air exchange fluxes of mercury could be enhanced by 207.1%, 32.4%, and 5.8%, respectively. This study elucidated the role of anthropogenic emissions in shaping the marine atmospheric mercury and the modulation of sea-air exchange fluxes, thereby informing valuable assessments regarding the influence of future reduced anthropogenic mercury emissions on the marine mercury cycle and ecosystems.

## 1. Introduction

Mercury is a ubiquitous toxic pollutant that can cycles among atmospheric, aquatic, and terrestrial environments (Mason et al., 2012; Lamborg et al., 2014). Anthropogenic discharge of mercury can be transported into marine atmospheres, subsequently entering oceans via wet and dry depositions, constituting a primary source of marine mercury (Outridge et al., 2018). A fraction of mercury that enters oceans can undergo methylation and bioaccumulate in the food chain, thereby posing health risks to humans through the consumption of methylmercury-contaminated seafood; another fraction converts to dissolved gaseous mercury and can escape from surface seawater through sea-air exchange processes (Lavoie et al., 2018; Obrist et al., 2018). This sea-air exchange is pivotal to the biogeochemical cycling of mercury, as it influences mercury concentrations in seawater, oceanic mercury accumulation rates, and methylmercury production (Mason et al., 2017; Ci et al., 2016). Simultaneously, the sea-air exchange of mercury represented the largest flux between different environmental media within the global mercury cycle. Previous estimates

https://doi.org/10.5194/egusphere-2025-623
Preprint. Discussion started: 21 February 2025


indicated that the release of gaseous elemental mercury from the global ocean contributed approximately one-third of the global atmospheric mercury emissions (Horowitz et al., 2017).

Numerous studies have emphasized the impact of anthropogenic sources on marine atmospheric mercury. For instance, one study conducted over the Bohai Sea revealed that the increased concentration of gaseous elemental mercury (GEM) resulted from the long-range transport of mercury released from anthropogenic sources (Wang et al., 2020). An island investigation over the East China Sea showed the outflow from mainland China was the primary contributor to atmospheric GEM (Fu et al., 2018). Cruises campaigns over the East China Sea and South China Sea observed elevated GEM concentrations at sites proximate to mainland China, indicating the prominent influence of terrestrial emissions (Fu et al., 2010; Wang et al., 2016a). Additionally, studies in the Gulf of Mexico, North Atlantic Ocean, and Mediterranean Sea also attributed significant portions of atmospheric mercury to anthropogenic emissions (Obrist et al., 2018). However, these studies primarily provided qualitative assessments without quantitatively elucidating the contribution of anthropogenic sources to marine atmospheric mercury. Although annual global anthropogenic atmospheric mercury emissions have been approximated to reach 2300 tons, accounting for about one-third of global atmospheric mercury emission (Pirrone et al., 2010; Zhang et al., 2016), the specific contributions to marine atmospheric mercury remained poorly delineated, thereby constraining insights into the oceanic mercury cycling dynamics. In this regard, it is imperative to develop methodologies capable of quantifying the contributions from anthropogenic sources to marine atmospheric mercury, particularly in critical marginal seas, which served as essential biogeochemical interfaces between landmasses and open oceans. Previous studies have indicated that the importance of the mercury cycling in offshore ecosystems approximated that within open oceanic environments (Fitzgerald et al., 2007). Marginal seas functioned not only as natural sinks for terrestrial mercury but also represented significant sources of atmospheric mercury (Ci et al., 2011). Given that China ranks as the foremost global emitter of anthropogenic atmospheric mercury (Pacyna et al., 2016; Pacyna et al., 2010; Zhang et al., 2015), its emissions inevitably exert profound influences on adjacent marginal seas.

Anthropogenic inputs influenced not only the concentrations of atmospheric mercury but also the dynamics of mercury sea-air exchange. Given that $Hg^0$ in the surface oceanic waters frequently

https://doi.org/10.5194/egusphere-2025-623
Preprint. Discussion started: 21 February 2025


exceeded its saturation levels, the prevailing direction of sea-air exchange was predominantly upward, facilitating the efflux of mercury from the ocean to the atmosphere (Andersson et al., 2008b; Mason et al., 2001; Huang and Zhang, 2021). The sea-air exchange of $Hg^0$ was governed by the concentration gradients at the atmosphere-seawater interface (Soerensen et al., 2013), which were influenced by the spectrum of physical and chemical processes within seawater, as well as meteorological conditions and ambient GEM concentrations (Costa and Liss, 1999; Mason, 2009; Selin, 2009). Previous studies illuminated the direct impact of dissolved gaseous mercury (DGM) in surface waters on $Hg^0$ fluxes, while photochemical reduction of Hg (II) has been identified as the principal mechanism driving the DGM generation in marine settings (Amyot et al., 1994; Huang and Zhang, 2021). Field measurements observed nocturnal peaks in DGM and $Hg^0$ fluxes, implying that dark reduction processes may significantly contribute to these dynamics (O'driscoll et al., 2003; Fu et al., 2013). $Hg^0$ fluxes increased 2-4 folds as a result of strengthened wind speeds coupled with Hg (II) inputs from atmospheric precipitation in the Intertropical Convergence Zone (ITCZ) region (Soerensen et al., 2014). While considerable research has elucidated the factors influencing the mercury sea-air exchange, few studies have comprehensively explored the repercussions of fluctuating GEM concentrations on $Hg^0$ sea-air dynamics. Given the backdrop of observed annual declines in GEM concentrations( $-0.011 \pm 0.006$ ng $m^{-3}$ $y^{-1}$) across most Northern Hemispheric regions from 2005 to 2020 (Feinberg et al., 2024) and particularly pronounced declines (-0.29 ng $m^{-3}$) in China from 2013 to 2017 (Liu et al., 2019), conducting such study in marginal seas is essential.

Under the influence of Chinese mainland emissions, mercury pollution in its adjacent marginal seas, such as the East China Sea, Yellow Sea, and Bohai Sea, exhibited pronounced severity. The East China Sea and Yellow Sea, as semi-enclosed seas, are located in the downwind region of East Asia and serve as a major pathway for the transport of pollutants to the Pacific Ocean. The Bohai Sea, as an inland sea, has received a substantial amount of pollutants from the Chinese mainland, making it one of the most mercury-polluted seas in the world (Luo et al., 2012). By focusing on the marginal seas surrounding China, this study integrated observations from two offshore islands, one research cruise, and a coastal city, to reveal the spatiotemporal distribution characteristics of total gaseous mercury (TGM) and dissolved gaseous mercury (DGM). The impact of oceanic

https://doi.org/10.5194/egusphere-2025-623
Preprint. Discussion started: 21 February 2025


meteorological conditions on the atmospheric mercury over the ocean was explored, particularly examining the effects of anthropogenic sources transported from the mainland. Furthermore, we developed a method to quantify the contributions from anthropogenic sources to marine atmospheric mercury and ultimately assessed how these inputs shaped the mercury sea-air exchange dynamics.

## 2. Methods

### 2.1 Study area

The study area, illustrated in Figure 1a, encompasses the Bohai Sea (BS), the Yellow Sea (YS), and the East China Sea (ECS). The BS, a shallow inner sea bordered by Liaoning, Hebei, and Shandong provinces, covers around $77\times10^3$ km$^2$. The YS, situated between mainland China and the Korean Peninsula, covers around $38\times10^4$ km$^2$. The ECS, a semi-enclosed marginal sea positioned downwind of East Asia, extends over $77\times10^4$ km$^2$. Field measurements were conducted at Juehua Island (JHI) in the BS, approximately 10 km from Xingcheng City, Liaoning Province. Due to its proximity to the mainland, JHI experienced marked impacts from anthropogenic emissions (Li et al., 2023). Field measurements were also conducted at Huaniao Island (HNI) in the ECS, approximately 80 km from Shanghai. Although local anthropogenic emissions were negligible there, this island was frequently affected by terrestrial transport during winter and spring, when prevailing northwesterly winds dominated (Fu et al., 2018; Qin et al., 2016). A cruise campaign was conducted aboard the research vessel (R/V) *Dongfanghong III*. The cruise routes, as shown in Figure 1a, covered most of the YS and ECS regions. Land-based measurements were conducted at a super site (Dianshan Lake, DSL) in the rural Shanghai Qingpu District. This super site is located at the intersection of Shanghai, Zhejiang, and Jiangsu provinces.

https://doi.org/10.5194/egusphere-2025-623
Preprint. Discussion started: 21 February 2025


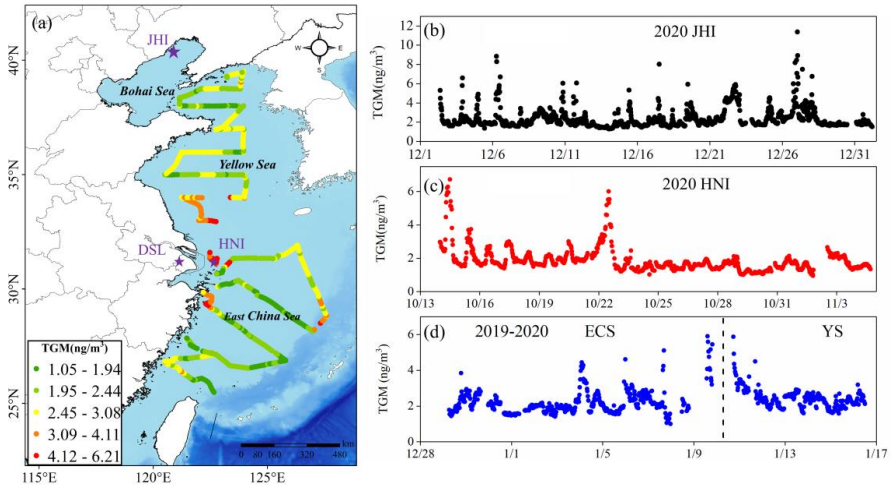


**Figure 1.** (a) The locations of two island sites (JHI and HNI) and one inland site (DSL) denoted by purple pentagrams. The spatial distribution of TGM concentrations over the East China Sea (ECS) and the Yellow Sea (YS) is shown along the cruise routes. The time series of TGM concentrations are measured at (b) JHI, (c) HNI, and (d) ECS+YS, respectively.

### 2.2 TGM/GEM measurements

TGM measurements were performed utilizing a modified Tekran 2600 instrument across various locations and timeframes, i.e., JHI from December 2, 2020 to January 1, 2021, HNI from October 14 to November 4, 2020, and aboard the research vessel (R/V) *Dongfanghong III* from December 29, 2019 to January 16, 2020. The Tekran 2600 monitor operated similarly to Tekran 2537B, which is widely used for continuous collection and analysis of atmospheric mercury (Sprovieri et al., 2016; Landis and Keeler, 2002). In this Tekran 2600 setup, sampling air passed through a Teflon filter to remove particulate matters, thereafter passing through a drying tube filled with soda lime to eradicate moisture prior to TGM collection in a gold tube. Following sample acquisition, the gold tube was heated to release Hg, which was subsequently analyzed using cold vapor atomic fluorescence spectroscopy (CVAFS) with argon as the carrier gas. Sampling intervals and flow rates were preset at 30 min and 500 ml/min, respectively. Calibration of the instrument was performed using the external calibration unit Terkan 2505 every 24 hours, ensuring that measured recovery rates exceeded 95% during each calibration cycle. Additionally, the drying tube

https://doi.org/10.5194/egusphere-2025-623
Preprint. Discussion started: 21 February 2025


and Teflon filter underwent replacement bi-weekly to maintain optimal performance.

GEM measurements were conducted at DSL in Shanghai from March 1, 2015 to February 28, 2019, employing the atmospheric mercury monitoring system (Tekran 2537B/1130/1135) as documented in our prior study (Qin et al., 2020). Briefly, GEM was captured utilizing dual gold cartridges at a flow rate of 1.0 LPM and 5-minute intervals. Subsequently, GEM underwent thermal decomposition for detection via CVAFS. During the sampling process, rigorous quality controls were applied. Prior to sampling, denuders and quartz filters were duly prepared and cleansed adhered to Tekran technical directives. To ensure accuracy, calibration was routinely executed every 47 hours using an internal permeation source, alongside manual injections of standard saturated mercury vapor. Further, the KCl-coated denuder, Teflon-coated glass inlet, and impactor plate were swapped weekly, while the quartz filters underwent monthly replacement.

It is noteworthy that TGM in the atmosphere comprises GEM and GOM (gaseous oxidized mercury). Generally, GEM constitutes over 95% of atmospheric mercury (Mao et al., 2016), particularly in the marine boundary layer, including China's marginal seas (Wang et al., 2016b; Fu et al., 2018; Ci et al., 2011; Wang et al., 2019a). Therefore, this study does not differentiate between TGM and GEM, conforming to analogous treatments in existing research (Fu et al., 2018; Ci et al., 2011).

### 2.3 DGM measurement

DGM (dissolved gaseous mercury) collection from seawater adhered to the procedure described in previous studies (Gardfeldt et al., 2003; O'driscoll et al., 2003). The sampling process involved the following steps. 1.5 L of surface seawater was collected in a Teflon bottle and subsequently transferred into a borosilicate glass bottle. An introduction of free-Hg argon at approximately 500 ml/min purged the seawater for 60 minutes to extract the DGM onto a gold trap, aided by a soda lime tube deployed to extract water vapor prior to the gold trap. The gold trap was maintained at ~50°C during extraction to prevent water vapor condensation. The DGM stored in the gold trap was measured using the Tekran 2600 post-sampling. To assure quality, stringent assurance and control measures were enacted through replicated field blank experiments. DGM excised from an equivalent volume of Milli-Q water served as the analytical system blank, encompassing a total

https://doi.org/10.5194/egusphere-2025-623
Preprint. Discussion started: 21 February 2025


of 12 blank experiments during field samplings at JHI and HNI, as well as during the R/V measurements. The mean system blank calculated was 2.5±1.3 pg/L (n = 20), with a detection limit of 3.4 pg/L.

**2.4 Ancillary data**

At JHI, water-soluble ions in $PM_{2.5}$, including sulphate ($SO_4^{2-}$), nitrate ($NO_3^-$), ammonium ($NH_4^+$), chloride ($Cl^-$), sodium ($Na^+$), potassium ($K^+$), magnesium ($Mg^{2+}$), calcium ($Ca^{2+}$), alongside the soluble gases such as ammonia ($NH_3$) and sulfur dioxide ($SO_2$) were continuously monitored using an In-situ Gas and Aerosol Composition monitoring system (IGAC) (Wang et al., 2022). Black carbon (BC) in $PM_{2.5}$ was measured continuously using a multi-wavelength Aethalometer (AE-33, Magee Scientific, USA). Meteorological data (e.g., air temperature, wind speed/direction) were observed using a co-located Pulsed Coherent Doppler Lidar (PCDL, Wind3D 6000) and a temperature/humidity sensor (YGC-BYX-M). The surface seawater temperature was measured by a salinity, conductivity and temperature meter (YSI EC300).

At HNI, meteorological parameters were gathered using an automatic weather station (AWS). Methods for analyzing BC and the surface seawater temperature mirrored those employed at JHI.

During the cruise campaign, the meteorological metrics (e.g., air temperature, wind speed/direction) and surface seawater temperature were collected from the instrumentations onboard the R/V. AE-33 was also used for BC measurements during the cruise.

**2.5 Positive matrix factorization (PMF)**

The PMF model is recognized for its efficacy in elucidating sources profiles and quantifying source contributions (Gibson et al., 2015). The underlying principle of PMF posits that sample concentration is dictated by source profiles with disparate contributions, mathematically represented as:

$$X_{ij} = \sum_{k=1}^{P} g_{ik} f_{kj} + e_{ij} \quad (1)$$

where $Xij$ represents the concentration of the $j$th species in the $i$th sample, $g_{ik}$ is the contribution of the $k$th factor in the $i$th sample, $f_{kj}$ provides the information about the mass fraction of the $j$th species in the $k$th factor, $e_{ij}$ is the residual for specific measurement, and $P$ represents the number of factors.

https://doi.org/10.5194/egusphere-2025-623
Preprint. Discussion started: 21 February 2025


Detail description can be seen in the previous study (Qin et al., 2020).

### 2.6 Sea-air exchange flux

The sea-air exchange fluxes of $Hg^0$ were calculated via the following equation (Andersson et al., 2008a; Wanninkhof and Oceans, 1992; Wangberg et al., 2001):

$$F = K_W(C_W - C_a/H') \quad (2)$$

where F is the sea-air exchange flux, $K_w$ represents the gas exchange velocity, $C_w$ and $C_a$ represent the DGM concentration in seawater and the TGM concentration in the atmosphere, respectively, H' is the dimensionless Henry's law coefficient of $Hg^0$ between the atmosphere and seawater. $K_w$ is calculated as follows (Soerensen et al., 2010b; Nightingale et al., 2000).

$$K_w = 0.31u_{10}^2(S_{C_{Hg}}/660)^{-0.5} \quad (3)$$

where $u_{10}$ is 10-meter wind speed, $S_{C_{Hg}}$ is the Schmidt number of $Hg^0$, 660 is the Schmidt number of $CO_2$ in 20 ℃ seawater (Poissant et al., 2000). H' is calculated as follows (Andersson et al., 2008a).

$$H' = \exp(-2403.3/T + 6.92) \quad (4)$$

Where T is the surface seawater temperature in K.

## 3. Results and Discussions

### 3.1 Characteristics of TGM over Chinese marginal seas

Figure 1b-d shows the time series of TGM concentrations measured during three field campaigns, including December 2, 2020 to January 1, 2021 at Juehua Island (JHI), October 14, 2020 to November 4, 2020 at Huaniao Island (HNI), and December 29, 2019 to January 16, 2020 over the Yellow Sea and East China Sea (YS/ECS). The mean TGM concentrations during the three periods were 2.32 ± 1.02 ng/m$^3$, 1.85 ± 0.74 ng/m$^3$, and 2.25 ± 0.66 ng/m$^3$, respectively. TGM at JHI exhibited pronounced fluctuations, frequently surpassing high values of 6 ng/m$^3$, which was attributed to the enhanced coal combustion for residential heating in winter (Li et al., 2023). Conversely, TGM at HNI and across the YS/ECS demonstrated less fluctuations, with concentrations predominantly remaining below 6 ng/m$^3$. The cruise campaign unveiled the spatial

https://doi.org/10.5194/egusphere-2025-623
Preprint. Discussion started: 21 February 2025


distribution of TGM over the ocean (Figure 1a), generally showing its decreasing trend with the increased distance away from the continent. Specifically, hot spots were observed in the eastern oceanic region of Jiangsu province, the Changjiang estuary, and the outer sea close to the Hangzhou Bay. The continental outflows likely explained this phenomenon. The mean TGM concentrations reached 2.36 ± 0.65 ng/m$^3$ and 2.16 ± 0.81 ng/m$^3$ over the Yellow Sea and East China Sea, respectively, significantly higher than the background level in the Northern Hemisphere (Sprovieri et al., 2016) and also surpassing measurements recorded in the other open ocean areas such as the South China Sea, Mediterranean Sea, Bering Sea, Pacific Ocean, and Atlantic Ocean (Laurier and Mason, 2007; Soerensen et al., 2010a; Mastromonaco et al., 2017; Kalinchuk et al., 2018; Wang et al., 2019b). 72h air mass backward trajectory analyses revealed that air masses over the YS predominantly originated from Liaoning and Inner Mongolia province in northern China, whereas trajectories over the ECS were largely dispersed across the ocean and Eastern China (Figure S1). This divergence elucidated the elevated TGM concentrations over the YS compared to the ECS.

The diurnal variations of TGM concentrations along with ambient temperature and sun flux during the three periods are displayed in Figure 2. At HNI, TGM commenced increasing at 7:00 a.m., peaking at around 2.44 ng/m$^3$ by 12:00, subsequently declining and stabilizing post 6:00 p.m. The mean TGM concentration during daytime (06:00-18:00) (2.00 ± 0.80 ng/m$^3$) surpassed that of nighttime (1.66 ± 0.40 ng/m$^3$) ($t$ test, $p < 0.001$). The TGM diurnal pattern displayed strong concordance with temperature and solar flux (Figure 2a), indicative of significant impacts from natural sources. At JHI (Figure 2b), TGM also rose around early morning and peaked at 2.65 ng/m$^3$ by 10:00 a.m., with nocturnal levels markedly increasing from 2.12 ng/m$^3$ at 6:00 p.m. to 2.60 ng/m$^3$ at 11:00 p.m. During daytime, TGM generally showed consistent variation with temperature and sun flux, indicating the influence of natural mercury release. However, the notable frequency of nocturnal peaks suggested that in addition to natural sources, TGM measured at JHI was also significantly affected by anthropogenic sources and unfavorable atmospheric diffusion conditions, specifically from coal combustion for the winter residential heating in northern China (Li et al., 2023). The diurnal pattern of TGM throughout the cruise campaign diverged from those of HNI and JHI, lacking a consistent relationship with temperature and sun flux. This was mainly due to that the cruise sampling was variable in both the temporal and spatial scale.

https://doi.org/10.5194/egusphere-2025-623
Preprint. Discussion started: 21 February 2025


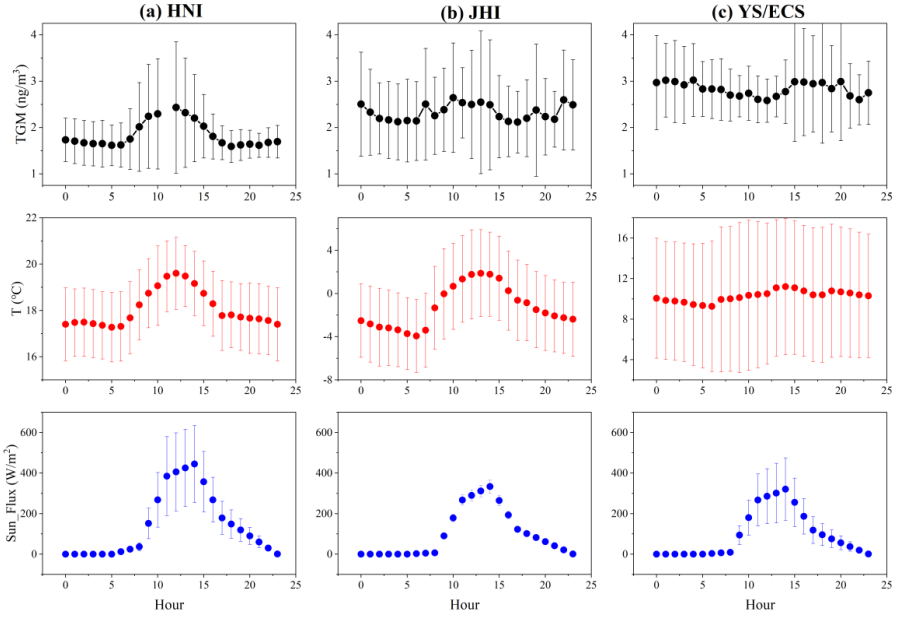


**Figure 2.** Diurnal variations of TGM, ambient temperature and sun flux at (a) HNI, (b) JHI, and (c) the YS/ECS cruise, respectively.

Positive correlations between TGM concentrations and ambient temperature at both HNI and JHI were observed, yielding $R^2$ values of 0.53 and 0.60, respectively (Figure 3a&3b). Since temperature played a crucial role in $Hg^0$ release from natural surfaces (Qin et al., 2020; Zhu et al., 2016a; Qin et al., 2019; Pannu et al., 2014), the evident correlation between TGM and temperature exemplified the significant effects of natural surface emissions.

Positive correlations were also observed between TGM, relative humidity, and wind speed at both HNI and JHI (Figure 3). Previous studies suggested wetting processes may promote the reduction of $Hg^{II}$ to $Hg^0$ in soil and water, while high wind speed favored the escape of $Hg^0$ from soils (Lin et al., 2010; Wanninkhof and Oceans, 1992; Pannu et al., 2014). Thus, relative humidity and wind speed were verified as critical factors influencing to the levels of TGM as similar as temperature.

At HNI, TGM increased concurrently with rising Planetary Boundary Layer (PBL) heights from around 380 to 1000 m, yet decreased with further increase in PBL beyond around 1000 m

https://doi.org/10.5194/egusphere-2025-623
Preprint. Discussion started: 21 February 2025


(Figure 3a). This was likely due to that the gradual increase in the PBL height from night to day corresponded with amplifying natural surface emissions of mercury. When PBL was below around 1km, the dilution effect due to heightened PBL could not counterbalance the enhanced natural surface emissions. In contrast, the similar phenomenon lacked manifestation at JHI, where TGM concentrations decreased with the increase of PBL (Figure 3b). This was likely ascribed to that the natural release around JHI was weaker than that around HNI, thus the dilution effect of elevated PBL overwhelmed the effect of natural surface emissions. Compared to HNI and JHI, the cruise campaign showed almost no relationship between TGM and temperature, relative humidity, wind speed, or PBL height were identified (Figure 3c), which shared similar reasons as discussed in the diurnal variation of TGM.

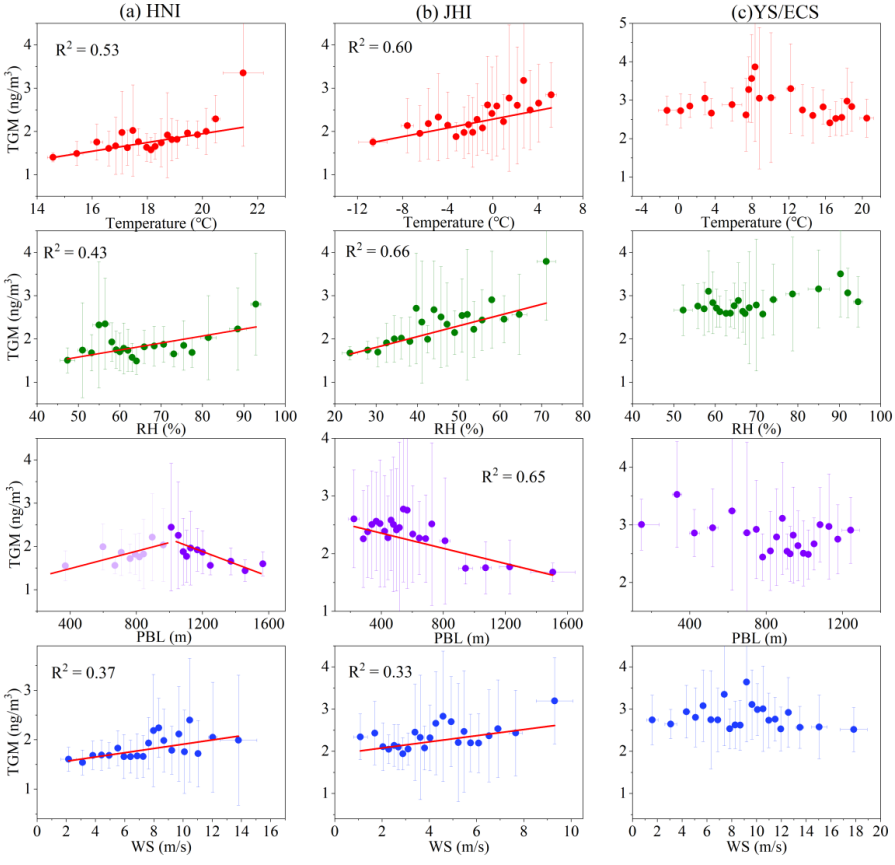


**Figure 3.** Relationship between TGM concentration and temperature, relative humidity, planetary

https://doi.org/10.5194/egusphere-2025-623
Preprint. Discussion started: 21 February 2025


boundary layer height, and wind speed at (a) HNI, (b) JHI, and (c)YS/ECS, respectively.

### 3.2 Influence of continental outflows on marine TGM

The potential source regions of TGM at HNI and JHI are illustrated in Figure S2. At HNI, TGM mainly derived from the lands of Jiangsu Province and vast coastal waters of the East China Sea. While at JHI, the hot spots of TGM were mainly located in the southern Mongolia and Beijing-Tianjin-Hebei regions. This indicated that the relatively high TGM concentrations at the coastal islands were closely related to the continental outflows. Using HNI as an example, Figure S3 compares the daily mean TGM concentration at HNI with the daily mean concentrations of CO, $SO_2$, and $PM_{2.5}$ in nearby coastal cities including Zhoushan, Ningbo, Jiaxing, Shanghai, and Ningbo. Consistently temporal variations were observed between TGM and these pollutants, particularly for the peak concentrations, further confirming that offshore TGM concentrations were significantly influenced by continental outflows.

To assess the impact of anthropogenic sources on marine TGM, the daily TGM concentrations at HNI and DSL (a suburban site in the Yangtze River Delta, Figure 1a) were compared (Figure 4a). Good consistency between them was found, indicating strong land-sea interactions. Furthermore, the correlation between TGM and BC at DSL was pronounced ($R^2$=0.56, Figure 4b). This was expected, as BC primarily originated from fossil fuels combustion (Li et al., 2021; Briggs and Long, 2016), which was also the major anthropogenic source of TGM. In contrast, the correlation between TGM and BC at HNI was much weaker ($R^2$=0.34, Figure 4c). Being an offshore site, HNI could be more strongly influenced by natural sources than DSL.

To qualitatively evaluate the relative importance of anthropogenic and natural sources to TGM, the ratio of TGM/BC was introduced as an indicator with lower ratios implying the prevalence of anthropogenic sources, and vice versa. Figure 4d shows that the TGM/BC ratio at DSL (mean of 1.6 ng $\mu g^{-1}$) was substantially lower than that at HNI (5.2 ng $\mu g^{-1}$), indicating much stronger contribution of natural sources to TGM in the coastal environment than the urban environment. The cruise measurement illustrated the spatial distribution of the TGM/BC ratio over YS/ECS, showing a tendency of decreasing values with increasing distance away from the coasts (Figure 4e). For instance, in the East China Sea, the TGM/BC ratio near the coasts typically ranged from 0.3 to 5.2

https://doi.org/10.5194/egusphere-2025-623
Preprint. Discussion started: 21 February 2025


ng $\mu g^{-1}$, while offshore values generally fluctuated between 8.6 and 22.9 ng $\mu g^{-1}$. This further corroborated the important contribution of marine natural emissions to TGM. In regard of different maritime spaces, the northern oceanic regions showed considerably lower values than those in the southern sea regions. In the Yellow Sea, the mean TGM/BC ratio was 4.1 ng $\mu g^{-1}$, noticeably lower than that of 6.5 ng $\mu g^{-1}$ observed in the East China Sea.

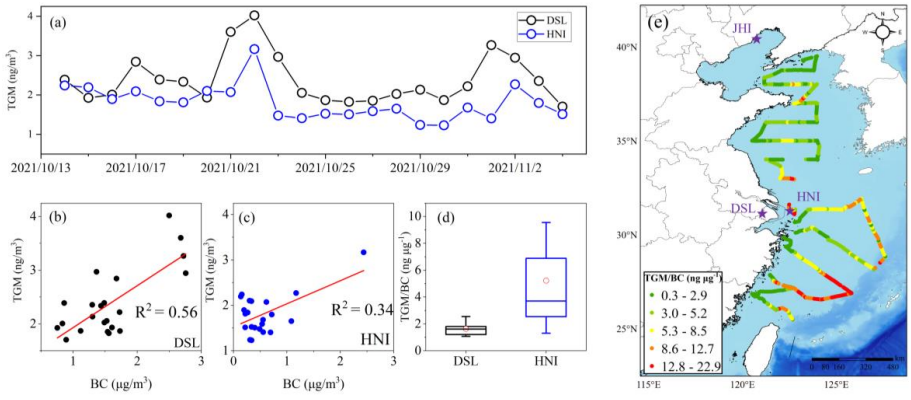


**Figure 4.** (a) Comparison of the daily TGM concentrations between DSL and HNI; Correlation between TGM and BC at (b) DSL and (c) HNI; (d) Comparison of the TGM/BC ratio between DSL and HNI; (e) Spatial distribution of the TGM/BC ratio along the cruise routes over the ECS and YS.

### 3.3 Quantification of anthropogenic vs. marine sources to TGM

Based on the discussions above, it is essential to disentangle the anthropogenic and natural sources of atmospheric mercury. Here, the PMF model was employed for the comprehensive dataset obtained at DSL and JHI, respectively. Considering the direct correlation between temperature and natural release of atmospheric mercury (Wang et al., 2014; Zhu et al., 2016b) and the indirect correlation between ammonia and natural release of atmospheric mercury (Qin et al., 2019), we utilized temperature and ammonia as indicators of natural atmospheric mercury sources, which has been proven feasible (Qin et al., 2020). Inputs for PMF also encompassed $SO_4^{2-}$, $Cl^-$, $NO_3^-$, $Na^+$, $NH_4^+$, $K^+$, $Mg^{2+}$, $Ca^{2+}$, $SO_2$, NO, Pb, Fe, K, Cr, Se, Ca, V, Mn, As, and Ni. While running the PMF model, we tested the number of factors from three to eight and determined the optimal solutions through analyzing the slope of the Q values in relation to the number of factors. The analyses

https://doi.org/10.5194/egusphere-2025-623
Preprint. Discussion started: 21 February 2025


revealed that a six-factor solution for DSL and a five-factor solution for JHI produced the most robust and coherent interpretations.

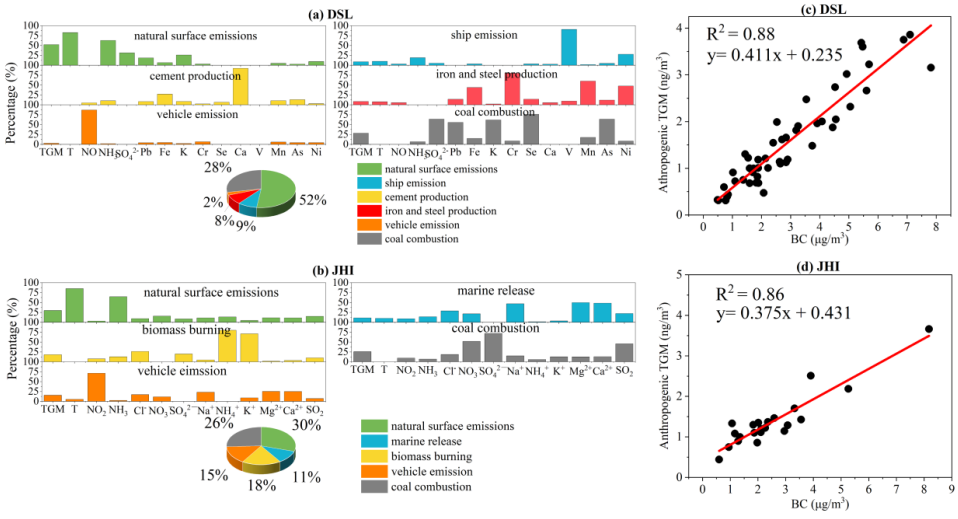


**Figure 5.** Source apportionment of TGM at (a) DSL and (b) JHI; Linear relationship between BC and anthropogenic TGM at (c) DSL and (d) JHI.

As detailed in Figure 5a, six distinct factors were resolved by PMF at DSL. The factor characterized by high loadings of temperature, $NH_3$, and TGM represented the natural surface emissions of mercury. A second factor with notable loading of V and moderate loading of Ni was ascribed to be shipping emissions. The cement production was associated with a factor exhibiting prominent Ca loading. The factor displaying high loading of Cr and moderate loadings of Fe and Mn was attributed to iron and steel production. Another factor, categorized by elevated NO levels, was linked to vehicle emissions. Finally, the factor with high loadings of $SO_4^{2-}$. Pb, K, Se, and As was indicative of coal combustion. PMF results indicated that the contributions of anthropogenic and natural sources to TGM were approximate 48% and 52% at DSL, respectively. By applying the same PMF modeling strategy at JHI, the contributions of anthropogenic and natural sources to TGM at JHI were 59% and 41%, respectively (Figure 5b). The source apportionment results signified substantial influences of both human and natural factors on TGM levels, with their contributions

https://doi.org/10.5194/egusphere-2025-623
Preprint. Discussion started: 21 February 2025


being nearly equivalent. Furthermore, correlation analysis was conducted between the absolute contribution of anthropogenic sources to GEM and BC, yielding a high correlation coefficient ($R^2$) of 0.88 and 0.86 at DSL and JHI (Figure 5c&5d), respectively. It should be noted that BC was not included in PMF modeling, thus the robust relationship between anthropogenic GEM and BC suggested that BC can serve as a viable indicator for quantifying anthropogenic contributions to TGM.

Based on the results above, the regression formulas obtained from DSL (TGM = 0.441*BC + 0.235, Figure 5c) and JHI (TGM = 0.375*BC + 0.431, Figure 5d) were further applied to the cruise observation for the purpose of differentiating the anthropogenic and natural fractions of TGM over the ocean. The following criteria were applied. If the air mass backward trajectories (purple segments in Figure S4) primarily originated from northern China, the JHI-derived formula was employed; If the air mass backward trajectories (green segments in Figure S4) passed through the Yangtze River Delta region or hovered over the East China Sea, the DSL-derived formula was enacted.

Time-series of mass concentrations of anthropogenic and natural TGM in different coastal and oceanic regions after applying the above equations are shown in Figure S5. Concentrations of anthropogenic TGM at HNI, JHI, ECS, and YS were 0.61 ± 0.29 ng/m$^3$, 1.28 ± 0.75 ng/m$^3$, 0.58 ± 0.44 ng/m$^3$, and 0.86 ± 0.22 ng/m$^3$, respectively. And the concentrations of natural TGM were 1.18 ± 0.48 ng/m$^3$, 0.88 ± 0.26 ng/m$^3$, 1.59 ± 0.53 ng/m$^3$, and 1.44 ± 0.53 ng/m$^3$ at the four locations above, respectively. To ensure the reliability of these results, the relationship between natural TGM and temperature was explored, yielding $R^2$ of 0.92, 0.76, 0.75, and 0.63 at HNI, JHI, ECS, and YS, respectively (Figure 6). The correlation was significantly stronger than that between the total TGM and temperature, particularly in the ECS and YS regions, where no correlations were observed (Figure 3c). This proved that the quantitative method established above was reliable.

https://doi.org/10.5194/egusphere-2025-623
Preprint. Discussion started: 21 February 2025


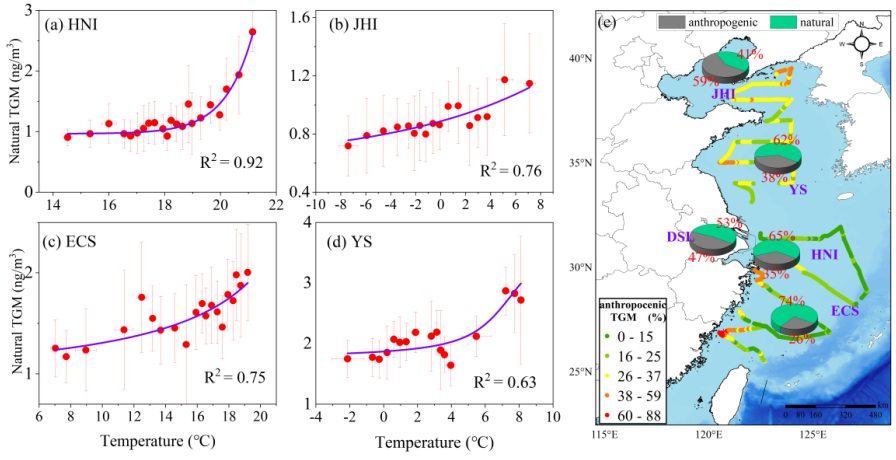


**Figure 6.** (a-d) Relationship between natural TGM and temperature at HNI, JHI, ECS, and YS, respectively. (e) Spatial distribution of the relative contributions of anthropogenic and natural sources to TGM concentrations along the cruise routes. The mean contributions over JHI, HNI, DSL, ECS, and YS are denoted by the pie charts.

The anthropogenic contributions to TGM along the cruise routes are plotted in Figure 6e, demonstrating significantly higher values near the coastal zones compared to the open ocean areas. In details, anthropogenic contributions to TGM near the East China Sea coastal zones reached as high as 60-88%, while the contributions diminished quickly to 15-25% over the open oceans. From the northern oceanic regions to the southern counterparts, the contribution of anthropogenic sources to TGM generally exhibited a decreasing trend, with values of around 59%, 38%, 35%, and 26% over JHI, YS, HNI, and ECS, respectively. The main cause of this phenomenon was that the Yellow Sea is a more enclosed maritime area compared to the East China Sea, making it more susceptible to terrestrial transport influences. In addition, during this cruise, the seawater temperature of the Yellow Sea was significantly lower than that of the East China Sea, which was unfavorable for the natural release of mercury.

### 3.4 Effects of anthropogenic inputs on the sea-air exchange of mercury

To determine the sea-air exchange flux of mercury, DGM (dissolved gaseous mercury)

https://doi.org/10.5194/egusphere-2025-623
Preprint. Discussion started: 21 February 2025


concentrations in seawater were measured at all sampling sites during the cruise (Figure S6). Figure S6 delineates the time-series of DGM observed at JHI, YS, HNI, and ECS, with mean concentrations of 21.3 ± 4.8, 29.9 ± 6.1, 42.0 ± 9.4, and 39.7 ± 10.9 pg/L, respectively. The DGM concentrations measured during this winter cruise campaign were significantly lower than those recorded previously during summer and fall in similar regions (Ci et al., 2011; Ci et al., 2015; Wang et al., 2016a), indicating a noticeable seasonal variation in DGM concentrations in the ECS and YS. Spatially, DGM concentrations in the ECS were higher than those in the YS, likely due to the significantly higher sea surface temperature in the ECS (mean: 14.8 ℃) compared to the YS (mean: 4.1 ℃) during the cruise campaign. Higher temperature was generally more favorable for the formation of DGM. Additionally, we observed that DGM concentrations were higher in coastal waters, particularly near the Yangtze River Estuary, where the concentration reached 51.4 pg/m³. This suggested that continental inputs, such as river discharge, had a significant influence on DGM levels in nearshore waters.

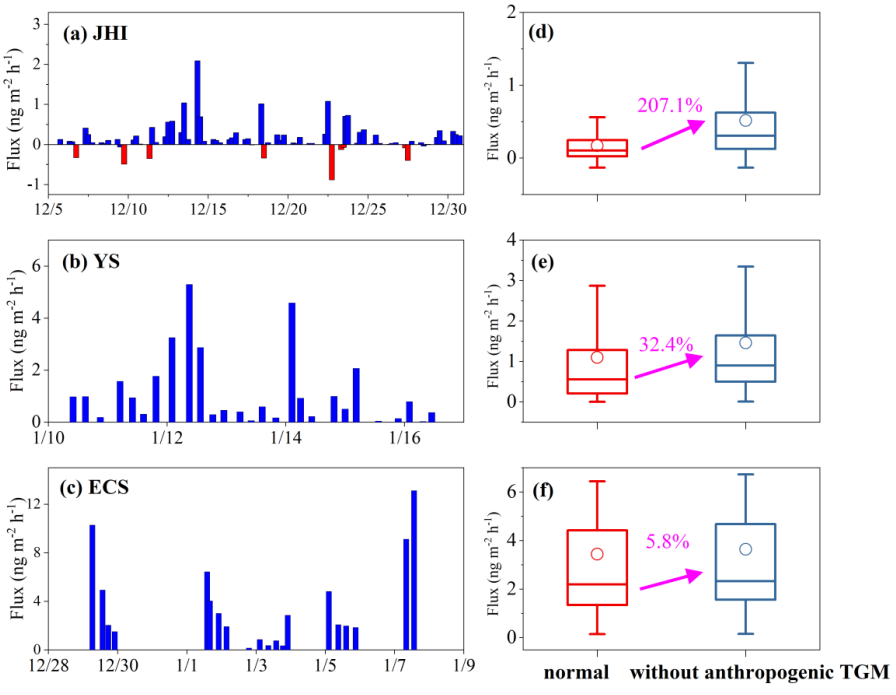

https://doi.org/10.5194/egusphere-2025-623
Preprint. Discussion started: 21 February 2025


**Figure 7.** (a-c) Sea-air exchange fluxes of mercury at JHI, YS, and ECS, respectively. (d-f) Comparison between the normal condition and the "without anthropogenic TGM" scenario, which represented recalculated sea-air exchange fluxes of mercury after subtracting the anthropogenic contributions of TGM concentrations.

Figure 7 shows the sea-air exchange fluxes of mercury within the BS (represented by JHI), YS, and ECS, which were 0.17±0.38, 1.10±1.34, and 3.44±3.24 ng $m^{-2}$ $h^{-1}$, respectively. It was evident that the $Hg^0$ fluxes during winter in the ECS was the highest, followed by the YS and the BS. BS acted as a weak mercury source region and even a mercury sink sometimes (negative flux in Figure 7a). Mercury fluxes observed during winter were lower than previous studies in other seasons, e.g., 4.6±3.6 ng $m^{-2}$ $h^{-1}$ in ECS during summer (Wang et al., 2016a), 3.07±3.03 ng $m^{-2}$ $h^{-1}$ in YS during spring (Wang et al., 2020), and 0.59±1.13 ng $m^{-2}$ $h^{-1}$ in BS during fall (Wang et al., 2020). To assess the impacts of anthropogenic inputs on the sea-air exchange, we recalculated the flux after removing the anthropogenic contributions from the TGM measurements. This recalculation revealed increases of mercury fluxes in all investigated oceanic regions with different extents. The post-adjustment mercury fluxes in the BS, YS, and ECS increased by 0.347, 0.357, and 0.199 ng $m^{-2}$ $h^{-1}$, respectively, corresponding to increased marine mercury emissions of 0.058, 0.308, and 0.332 tons, respectively. Compared to the normal condition, the BS exhibited the most substantial increase in marine mercury release (207.1%) following the deduction of anthropogenic impacts, suceeded by the YS (32.4%) and the ECS (5.8%) (Figure 7d-7f). These results quantitatively elucidated the impact of anthropogenic emissions on marine mercury release, underscoring the potential effects of diminished anthropogenic emissions on oceanic mercury cycling.

## 4. Conclusions and implications

This study elucidated the effects of anthropogenic sources on atmospheric mercury concentrations across various marginal seas and the subsequent influence on sea-air exchange dynamics of mercury. Through comprehensive observations across island, cruise, and terrestrial settings, we delineated atmospheric mercury distribution characteristics within the Chinese marginal seas. The relationships between TGM and various environmental parameters suggested the

https://doi.org/10.5194/egusphere-2025-623
Preprint. Discussion started: 21 February 2025


significance of natural sources in constraining oceanic atmospheric mercury levels. Notably, TGM peaks recorded at terrestrial and island sites exemplified the influence of continental outflows on the marine TGM. The introduction of the TGM/BC ratio functioned as a qualitative proxy for assessing the extent of anthropogenic contributions. Furthermore, we articulated a quantitative methodology for assessing anthropogenic contributions to marine atmospheric mercury, revealing that these sources contributed 59%, 38%, and 26% to atmospheric mercury levels across the Bohai Sea, Yellow Sea, and East China Sea, respectively. The winter sea-air exchange fluxes of mercury in these three seas were estimated as 0.169, 1.100, and 3.442 ng $m^{-2}$ $h^{-1}$, respectively, with increases of 0.347, 0.357, and 0.199 ng $m^{-2}$ $h^{-1}$ subsequent to deducting anthropogenic contributions.

Conducting atmospheric mercury measurements over oceans presented considerable complexities compared to terrestrial observations, further compounded by challenges associated with determining atmospheric mercury sources in the oceanic environment. This study established a quantitative method grounded in extensive observations encompassing terrestrial, island, and marine contexts, facilitating estimations of anthropogenic contributions to atmospheric mercury solely predicated on atmospheric mercury and black carbon data. This methodology may offer valuable insights for analogous analyses of atmospheric mercury and other pollutants across diverse oceanic regions globally. Using this method, we further quantified the extent to which anthropogenic sources suppressed the sea-air exchange of mercury. Against the backdrop of declining global anthropogenic atmospheric mercury emissions over the past 30 years, our findings suggested an increase in mercury release from the ocean. Consequently, the mercury content in the ocean will be likely to decrease, resulting in less inorganic mercury available for methylmercury production. These insights contribute to a deeper understanding of the biogeochemical cycle of mercury and enhance our ability to evaluate its impacts on marine ecosystems and human health.

**Data Availability Statement**

The raw data generated in this study have been uploaded to Zenodo (https://doi.org/10.5281/zenodo.14847622).

**Author contributions**

https://doi.org/10.5194/egusphere-2025-623
Preprint. Discussion started: 21 February 2025


KH designed this study. XQ, HL, JC, XW, GW, CL, DL, JH, and YL performed data collection. XQ and KH performed data analysis and wrote the paper. All have commented on and reviewed the paper.

**Competing interests**

The authors declare that they have no conflict of interest.

**Acknowledgments**

This work was financially supported by the National Key R&D Plan Programs (2023YFE0102500, 2018YFC0213105) and the National Science Foundation of China (42175119, 42361144711). Junjie Wei, Hao Ding, and Qiongzhen Wang acknowledge financial support from Central Guiding Local Science and Technology Development Fund Projects (No.2023ZY1024).

**References:**

Amyot, M., Mierle, G., Lean, D. R. S., and McQueen, D. J.: SUNLIGHT-INDUCED FORMATION OF DISSOLVED GASEOUS MERCURY IN LAKE WATERS, Environmental science & technology, 28, 2366-2371, 10.1021/es00062a022, 1994.

Andersson, M. E., Gårdfeldt, K., Wängberg, I., and Strömberg, D.: Determination of Henry's law constant for elemental mercury, Chemosphere, 73, 587-592, https://doi.org/10.1016/j.chemosphere.2008.05.067, 2008a.

Andersson, M. E., Sommar, J., Gårdfeldt, K., and Lindqvist, O.: Enhanced concentrations of dissolved gaseous mercury in the surface waters of the Arctic Ocean, Mar. Chem., 110, 190-194, 10.1016/j.marchem.2008.04.002, 2008b.

Briggs, N. L. and Long, C. M.: Critical review of black carbon and elemental carbon source apportionment in Europe and the United States, Atmospheric Environment, 144, 409-427, 10.1016/j.atmosenv.2016.09.002, 2016.

Ci, Z., Wang, C., Wang, Z., and Zhang, X.: Elemental mercury (Hg(0)) in air and surface waters of the Yellow Sea during late spring and late fall 2012: Concentration, spatial-temporal distribution and air/sea flux, Chemosphere, 119, 199-208, https://doi.org/10.1016/j.chemosphere.2014.05.064, 2015.

Ci, Z. J., Zhang, X. S., Yin, Y. G., Chen, J. S., and Wang, S. W.: Mercury Redox Chemistry in Waters of the Eastern Asian Seas: From Polluted Coast to Clean Open Ocean, Environmental science & technology, 50, 2371-2380, 10.1021/acs.est.5b05372, 2016.

Ci, Z. J., Zhang, X. S., Wang, Z. W., Niu, Z. C., Diao, X. Y., and Wang, S. W.: Distribution and air-sea exchange of mercury (Hg) in the Yellow Sea, Atmospheric Chemistry and Physics, 11, 2881-2892, 10.5194/acp-11-2881-2011, 2011.

Costa, M. and Liss, P. S.: Photoreduction of mercury in sea water and its possible implications for Hg0 air–sea fluxes, Mar. Chem., 68, 87-95, https://doi.org/10.1016/S0304-4203(99)00067-5, 1999.

https://doi.org/10.5194/egusphere-2025-623
Preprint. Discussion started: 21 February 2025


Feinberg, A., Selin, N. E., Braban, C. F., Chang, K.-L., Custodio, D., Jaffe, D. A., Kyllonen, K., Landis, M. S., Leeson, S. R., Luke, W., Molepo, K. M., Murovec, M., Nerentorp Mastromonaco, M. G., Aspmo Pfaffhuber, K., Rudiger, J., Sheu, G.-R., and St Louis, V. L.: Unexpected anthropogenic emission decreases explain recent atmospheric mercury concentration declines, Proceedings of the National Academy of Sciences of the United States of America, 121, e2401950121, 10.1073/pnas.2401950121, 2024.

Fitzgerald, W. F., Lamborg, C. H., and Hammerschmidt, C. R.: Marine Biogeochemical Cycling of Mercury, Chemical Reviews, 107, 641-662, 10.1021/cr050353m, 2007.

Fu, X., Yang, X., Tan, Q., Ming, L., Lin, T., Lin, C.-J., Li, X., and Feng, X.: Isotopic Composition of Gaseous Elemental Mercury in the Marine Boundary Layer of East China Sea, Journal of Geophysical Research: Atmospheres, 10.1029/2018jd028671, 2018.

Fu, X. W., Feng, X. B., Yin, R. S., and Zhang, H.: Diurnal variations of total mercury, reactive mercury, and dissolved gaseous mercury concentrations and water/air mercury flux in warm and cold seasons from freshwaters of southwestern China, Environ. Toxicol. Chem., 32, 2256-2265, 10.1002/etc.2323, 2013.

Fu, X. W., Feng, X. B., Zhang, G., Xu, W. H., Li, X. D., Yao, H., Liang, P., Li, J., Sommar, J., Yin, R. S., and Liu, N.: Mercury in the marine boundary layer and seawater of the South China Sea: Concentrations, sea/air flux, and implication for land outflow, J. Geophys. Res.-Atmos., 115, 11, 10.1029/2009jd012958, 2010.

Gardfeldt, K., Sommar, J., Ferrara, R., Ceccarini, C., Lanzillotta, E., Munthe, J., Wangberg, I., Lindqvist, O., Pirrone, N., Sprovieri, F., Pesenti, E., and Stromberg, D.: Evasion of mercury from coastal and open waters of the Atlantic Ocean and the Mediterranean Sea, Atmospheric Environment, 37, S73-S84, 10.1016/s1352-2310(03)00238-3, 2003.

Gibson, M. D., Haelssig, J., Pierce, J. R., Parrington, M., Franklin, J. E., Hopper, J. T., Li, Z., and Ward, T. J.: A comparison of four receptor models used to quantify the boreal wildfire smoke contribution to surface PM<sub>2.5</sub> in Halifax, Nova Scotia during the BORTAS-B experiment, Atmos. Chem. Phys., 15, 815-827, 10.5194/acp-15-815-2015, 2015.

Horowitz, H. M., Jacob, D. J., Zhang, Y., Dibble, T. S., Slemr, F., Amos, H. M., Schmidt, J. A., Corbitt, E. S., Marais, E. A., and Sunderland, E. M.: A new mechanism for atmospheric mercury redox chemistry: implications for the global mercury budget, Atmospheric Chemistry and Physics, 17, 6353-6371, 10.5194/acp-17-6353-2017, 2017.

Huang, S. and Zhang, Y.: Interannual Variability of Air-Sea Exchange of Mercury in the Global Ocean: The "Seesaw Effect" in the Equatorial Pacific and Contributions to the Atmosphere, Environmental science & technology, 55, 7145-7156, 10.1021/acs.est.1c00691, 2021.

Kalinchuk, V. V., Mishukov, V. F., and Astakhov, A. S.: Arctic source for elevated atmospheric mercury (Hg-0) in the western Bering Sea in the summer of 2013, Journal of Environmental Sciences, 68, 114-121, 10.1016/j.jes.2016.12.022, 2018.

Lamborg, C. H., Hammerschmidt, C. R., Bowman, K. L., Swarr, G. J., Munson, K. M., Ohnemus, D. C., Lam, P. J., Heimburger, L. E., Rijkenberg, M. J., and Saito, M. A.: A global ocean inventory of anthropogenic mercury based on water column measurements, Nature, 512, 65-68, 10.1038/nature13563, 2014.

Landis, M. S. and Keeler, G. J.: Atmospheric mercury deposition to Lake Michigan during the Lake Michigan Mass Balance Study, Environmental science & technology, 36, 4518-4524, 10.1021/es011217b, 2002.

Laurier, F. and Mason, R.: Mercury concentration and speciation in the coastal and open ocean boundary

https://doi.org/10.5194/egusphere-2025-623
Preprint. Discussion started: 21 February 2025


layer, J. Geophys. Res.-Atmos., 112, 10.1029/2006jd007320, 2007.
Lavoie, R. A., Bouffard, A., Maranger, R., and Amyot, M.: Mercury transport and human exposure from global marine fisheries, Scientific reports, 8, 10.1038/s41598-018-24938-3, 2018.
Li, H., Huang, K., Fu, Q., Lin, Y., Chen, J., Deng, C., Tian, X., Tang, Q., Song, Q., and Wei, Z.: Airborne black carbon variations during the COVID-19 lockdown in the Yangtze River Delta megacities suggest actions to curb global warming, Environ Chem Lett, 1-10, 10.1007/s10311-021-01327-3, 2021.
Li, H., Qin, X. F., Chen, J., Wang, G. C., Liu, C. F., Lu, D., Zheng, H. T., Song, X. Q., Gao, Q. Q., Xu, J., Zhu, Y. C., Liu, J. G., Wang, X. F., Deng, C. R., and Huang, K.: Continuous Measurement and Molecular Compositions of Atmospheric Water-Soluble Brown Carbon in the Nearshore Marine Boundary Layer of Northern China: Secondary Formation and Influencing Factors, J. Geophys. Res.-Atmos., 128, 10.1029/2023jd038565, 2023.
Lin, C.-J., Gustin, M. S., Singhasuk, P., Eckley, C., and Miller, M.: Empirical Models for Estimating Mercury Flux from Soils, Environmental science & technology, 44, 8522-8528, 10.1021/es1021735, 2010.
Liu, K., Wu, Q., Wang, L., Wang, S., Liu, T., Ding, D., Tang, Y., Li, G., Tian, H., Duan, L., Wang, X., Fu, X., Feng, X., and Hao, J.: Measure-Specific Effectiveness of Air Pollution Control on China's Atmospheric Mercury Concentration and Deposition during 2013-2017, Environmental science & technology, 53, 8938-8946, 10.1021/acs.est.9b02428, 2019.
Luo, W., Wang, T., Jiao, W., Hu, W., Naile, J. E., Khim, J. S., Giesy, J. P., and Lu, Y.: Mercury in coastal watersheds along the Chinese Northern Bohai and Yellow Seas, Journal of Hazardous Materials, 215-216, 199-207, https://doi.org/10.1016/j.jhazmat.2012.02.052, 2012.
Mao, H., Cheng, I., and Zhang, L.: Current understanding of the driving mechanisms for spatiotemporal variations of atmospheric speciated mercury: a review, Atmos. Chem. Phys., 16, 12897-12924, 10.5194/acp-16-12897-2016, 2016.
Mason, R. P.: Mercury emissions from natural processes and their importance in the global mercury cycle, in: Mercury Fate and Transport in the Global Atmosphere: Emissions, Measurements and Models, edited by: Mason, R., and Pirrone, N., Springer US, Boston, MA, 173-191, 10.1007/978-0-387-93958-2_7, 2009.
Mason, R. P., Lawson, N. M., and Sheu, G. R.: Mercury in the Atlantic Ocean: factors controlling air–sea exchange of mercury and its distribution in the upper waters, Deep Sea Research Part II: Topical Studies in Oceanography, 48, 2829-2853, https://doi.org/10.1016/S0967-0645(01)00020-0, 2001.
Mason, R. P., Hammerschmidt, C. R., Lamborg, C. H., Bowman, K. L., Swarr, G. J., and Shelley, R. U.: The air-sea exchange of mercury in the low latitude Pacific and Atlantic Oceans, Deep-Sea Research Part I-Oceanographic Research Papers, 122, 17-28, 10.1016/j.dsr.2017.01.015, 2017.
Mason, R. P., Choi, A. L., Fitzgerald, W. F., Hammerschmidt, C. R., Lamborg, C. H., Soerensen, A. L., and Sunderland, E. M.: Mercury biogeochemical cycling in the ocean and policy implications, Environmental Research, 119, 101-117, 10.1016/j.envres.2012.03.013, 2012.
Mastromonaco, M. G. N., Gardfeldt, K., Assmann, K. M., Langer, S., Delali, T., Shlyapnikov, Y. M., Zivkovic, I., and Horvat, M.: Speciation of mercury in the waters of the Weddell, Amundsen and Ross Seas (Southern Ocean), Mar. Chem., 193, 20-33, 10.1016/j.marchem.2017.03.001, 2017.
Nightingale, P. D., Malin, G., Law, C. S., Watson, A. J., Liss, P. S., Liddicoat, M. I., Boutin, J., and Upstill-Goddard, R. C.: In situ evaluation of air-sea gas exchange parameterizations using novel conservative and volatile tracers, 14, 373-387, https://doi.org/10.1029/1999GB900091, 2000.
O'Driscoll, N. J., Beauchamp, S., Siciliano, S. D., Rencz, A. N., and Lean, D. R. S.: Continuous Analysis

https://doi.org/10.5194/egusphere-2025-623
Preprint. Discussion started: 21 February 2025


of Dissolved Gaseous Mercury (DGM) and Mercury Flux in Two Freshwater Lakes in Kejimkujik Park, Nova Scotia: Evaluating Mercury Flux Models with Quantitative Data, Environmental science & technology, 37, 2226-2235, 10.1021/es025944y, 2003.

Obrist, D., Kirk, J. L., Zhang, L., Sunderland, E. M., Jiskra, M., and Selin, N. E.: A review of global environmental mercury processes in response to human and natural perturbations: Changes of emissions, climate, and land use, Ambio, 47, 116-140, 10.1007/s13280-017-1004-9, 2018.

Outridge, P. M., Mason, R. P., Wang, F., Guerrero, S., and Heimbürger-Boavida, L. E.: Updated Global and Oceanic Mercury Budgets for the United Nations Global Mercury Assessment 2018, Environmental science & technology, 52, 11466-11477, 10.1021/acs.est.8b01246, 2018.

Pacyna, E. G., Pacyna, J. M., Sundseth, K., Munthe, J., Kindbom, K., Wilson, S., Steenhuisen, F., and Maxson, P.: Global emission of mercury to the atmosphere from anthropogenic sources in 2005 and projections to 2020, Atmospheric Environment, 44, 2487-2499, 10.1016/j.atmosenv.2009.06.009, 2010.

Pacyna, J. M., Travnikov, O., De Simone, F., Hedgecock, I. M., Sundseth, K., Pacyna, E. G., Steenhuisen, F., Pirrone, N., Munthe, J., and Kindbom, K.: Current and future levels of mercury atmospheric pollution on a global scale, Atmos. Chem. Phys., 16, 12495-12511, 10.5194/acp-16-12495-2016, 2016.

Pannu, R., Siciliano, S. D., and O'Driscoll, N. J.: Quantifying the effects of soil temperature, moisture and sterilization on elemental mercury formation in boreal soils, Environmental Pollution, 193, 138-146, 10.1016/j.envpol.2014.06.023, 2014.

Pirrone, N., Cinnirella, S., Feng, X., Finkelman, R. B., Friedli, H. R., Leaner, J., Mason, R., Mukherjee, A. B., Stracher, G. B., Streets, D. G., and Telmer, K.: Global mercury emissions to the atmosphere from anthropogenic and natural sources, Atmos. Chem. Phys., 10, 5951-5964, 10.5194/acp-10-5951-2010, 2010.

Poissant, L., Amyot, M., Pilote, M., and Lean, D.: Mercury Water−Air Exchange over the Upper St. Lawrence River and Lake Ontario, Environmental science & technology, 34, 3069-3078, 10.1021/es990719a, 2000.

Qin, X., Wang, F., Deng, C., Wang, F., and Yu, G.: Seasonal variation of atmospheric particulate mercury over the East China Sea, an outflow region of anthropogenic pollutants to the open Pacific Ocean, Atmos. Pollut. Res., 7, 876-883, 10.1016/j.apr.2016.05.004, 2016.

Qin, X., Wang, X., Shi, Y., Yu, G., Zhao, N., Lin, Y., Fu, Q., Wang, D., Xie, Z., Deng, C., and Huang, K.: Characteristics of atmospheric mercury in a suburban area of east China: sources, formation mechanisms, and regional transport, Atmos. Chem. Phys., 19, 5923-5940, 10.5194/acp-19-5923-2019, 2019.

Qin, X., Zhang, L., Wang, G., Wang, X., Fu, Q., Xu, J., Li, H., Chen, J., Zhao, Q., Lin, Y., Huo, J., Wang, F., Huang, K., and Deng, C.: Assessing contributions of natural surface and anthropogenic emissions to atmospheric mercury in a fast-developing region of eastern China from 2015 to 2018, Atmos. Chem. Phys., 20, 10985-10996, 10.5194/acp-20-10985-2020, 2020.

Selin, N. E.: Global Biogeochemical Cycling of Mercury: A Review, Annu. Rev. Environ. Resour., 34, 43-63, 10.1146/annurev.environ.051308.084314, 2009.

Soerensen, A. L., Mason, R. P., Balcom, P. H., and Sunderland, E. M.: Drivers of Surface Ocean Mercury Concentrations and Air–Sea Exchange in the West Atlantic Ocean, Environmental science & technology, 47, 7757-7765, 10.1021/es401354q, 2013.

Soerensen, A. L., Skov, H., Jacob, D. J., Soerensen, B. T., and Johnson, M. S.: Global Concentrations of Gaseous Elemental Mercury and Reactive Gaseous Mercury in the Marine Boundary Layer, Environmental science & technology, 44, 7425-7430, 10.1021/es903839n, 2010a.

Soerensen, A. L., Mason, R. P., Balcom, P. H., Jacob, D. J., Zhang, Y. X., Kuss, J., and Sunderland, E.

https://doi.org/10.5194/egusphere-2025-623
Preprint. Discussion started: 21 February 2025


M.: Elemental Mercury Concentrations and Fluxes in the Tropical Atmosphere and Ocean, Environmental science & technology, 48, 11312-11319, 10.1021/es503109p, 2014.

Soerensen, A. L., Sunderland, E. M., Holmes, C. D., Jacob, D. J., Yantosca, R. M., Skov, H., Christensen, J. H., Strode, S. A., and Mason, R. P.: An Improved Global Model for Air-Sea Exchange of Mercury: High Concentrations over the North Atlantic, Environmental science & technology, 44, 8574-8580, 10.1021/es102032g, 2010b.

Sprovieri, F., Pirrone, N., Bencardino, M., D'Amore, F., Carbone, F., Cinnirella, S., Mannarino, V., Landis, M., Ebinghaus, R., Weigelt, A., Brunke, E. G., Labuschagne, C., Martin, L., Munthe, J., Wangberg, I., Artaxo, P., Morais, F., de Melo Jorge Barbosa, H., Brito, J., Cairns, W., Barbante, C., Del Carmen Dieguez, M., Garcia, P. E., Dommergue, A., Angot, H., Magand, O., Skov, H., Horvat, M., Kotnik, J., Read, K. A., Neves, L. M., Gawlik, B. M., Sena, F., Mashyanov, N., Obolkin, V., Wip, D., Feng, X. B., Zhang, H., Fu, X., Ramachandran, R., Cossa, D., Knoery, J., Marusczak, N., Nerentorp, M., and Norstrom, C.: Atmospheric mercury concentrations observed at ground-based monitoring sites globally distributed in the framework of the GMOS network, Atmos Chem Phys, 16, 11915-11935, 10.5194/acp-16-11915-2016, 2016.

Wang, C., Wang, Z., and Zhang, X.: Characteristics of mercury speciation in seawater and emission flux of gaseous mercury in the Bohai Sea and Yellow Sea, Environ Res, 182, 109092, 10.1016/j.envres.2019.109092, 2020.

Wang, C., Ci, Z., Wang, Z., and Zhang, X.: Air-sea exchange of gaseous mercury in the East China Sea, Environ Pollut, 212, 535-543, 10.1016/j.envpol.2016.03.016, 2016a.

Wang, C., Wang, Z., Hui, F., and Zhang, X.: Speciated atmospheric mercury and sea–air exchange of gaseous mercury in the South China Sea, Atmospheric Chemistry and Physics, 19, 10111-10127, 10.5194/acp-19-10111-2019, 2019a.

Wang, C., Wang, Z., Hui, F., and Zhang, X.: Speciated atmospheric mercury and sea-air exchange of gaseous mercury in the South China Sea, Atmospheric Chemistry and Physics, 19, 10111-10127, 10.5194/acp-19-10111-2019, 2019b.

Wang, C., Wang, Z., Ci, Z., Zhang, X., and Tang, X.: Spatial-temporal distributions of gaseous element mercury and particulate mercury in the Asian marine boundary layer, Atmospheric Environment, 126, 107-116, 10.1016/j.atmosenv.2015.11.036, 2016b.

Wang, G. C., Chen, J., Xu, J., Yun, L., Zhang, M. D., Li, H., Qin, X. F., Deng, C. R., Zheng, H. T., Gui, H. Q., Liu, J. G., and Huang, K.: Atmospheric Processing at the Sea-Land Interface Over the South China Sea: Secondary Aerosol Formation, Aerosol Acidity, and Role of Sea Salts, J. Geophys. Res.-Atmos., 127, 10.1029/2021jd036255, 2022.

Wang, X., Lin, C. J., and Feng, X.: Sensitivity analysis of an updated bidirectional air-surface exchange model for elemental mercury vapor, Atmospheric Chemistry and Physics, 14, 6273-6287, 10.5194/acp-14-6273-2014, 2014.

Wangberg, I., Schmolke, S., Schager, P., Munthe, J., Ebinghaus, R., and Iverfeldt, A.: Estimates of air-sea exchange of mercury in the Baltic Sea, Atmospheric Environment, 35, 5477-5484, 10.1016/s1352-2310(01)00246-1, 2001.

Wanninkhof and Oceans, R. J. J. o. G. R.: Relationship between wind speed and gas exchange over the ocean, 97, 7373, 1992.

Zhang, L., Wang, S., Wang, L., Wu, Y., Duan, L., Wu, Q., Wang, F., Yang, M., Yang, H., Hao, J., and Liu, X.: Updated emission inventories for speciated atmospheric mercury from anthropogenic sources in China, Environmental science & technology, 49, 3185-3194, 10.1021/es504840m, 2015.

https://doi.org/10.5194/egusphere-2025-623
Preprint. Discussion started: 21 February 2025


706 Zhang, Y., Jacob, D. J., Horowitz, H. M., Chen, L., Amos, H. M., Krabbenhoft, D. P., Slemr, F., St Louis,
707 V. L., and Sunderland, E. M.: Observed decrease in atmospheric mercury explained by global decline in
708 anthropogenic emissions, Proc Natl Acad Sci U S A, 113, 526-531, 10.1073/pnas.1516312113, 2016.
709 Zhu, W., Lin, C.-J., Wang, X., Sommar, J., Fu, X., and Feng, X.: Global observations and modeling of
710 atmosphere–surface exchange of elemental mercury: a critical review, Atmospheric Chemistry and
711 Physics, 16, 4451-4480, 10.5194/acp-16-4451-2016, 2016a.
712 Zhu, W., Lin, C. J., Wang, X., Sommar, J., Fu, X., and Feng, X.: Global observations and modeling of
713 atmosphere–surface exchange of elemental mercury: a critical review, Atmos. Chem. Phys., 16, 4451-
714 4480, 10.5194/acp-16-4451-2016, 2016b.
715
716
717
718
719